

# Rigorous Analytical/Graphical Injection Locking Analysis of Two-Port Negative Resistance Oscillators

Ting Mei and Jaijeet Roychowdhury  
 {meiting, jr}@umn.edu  
 University of Minnesota, Twin Cities, USA

**Abstract**—In this paper, we present a simple but rigorous nonlinear analysis for understanding and predicting steady-state operation and injection locking in two-port nonlinear negative-resistance oscillators (such as the Colpitts, Pierce, etc., topologies commonly used in RFICs). Key advances of our approach include the use of vector-based nonlinear feedback analysis and treatment of amplitude and frequency components in a coupled way. We develop rigorous and insightful graphical approaches for output voltage estimation and injection lock range prediction. We validate our analytical approach against transient and harmonic balance simulations.

## I. INTRODUCTION

Oscillators are building blocks in analog, RF and mixed-signal systems. When perturbed by external signals, they often exhibit interesting and practically useful behaviors such as injection locking [1]. Injection locking is a nonlinear phenomena in which an oscillator changes its natural frequency to match the frequency of an externally injected signal. This phenomenon has attracted increasing interest for design purposes — for example, it has been used in PLL design to achieve fast lock without sacrificing other performance metrics [4]. It has also been exploited in frequency dividers [14, 17], quadrature oscillators [5], etc.. Therefore, understanding the phenomenon and predicting it correctly is an important problem.

A common approach for predicting injection locking is to use SPICE-level transient simulation. However, computationally, transient simulation can be extremely inaccurate and inefficient for oscillators (see, e.g., [8] for details). To alleviate transient simulation issues for oscillators, fast simulation techniques (e.g., [3, 7, 10]) have been developed and used for injection locking/pulling prediction. These methods, which are based on linearization, can become inaccurate as injection strength grows. From a designer's point of view, simulation techniques, though very useful for design, tend to provide relatively little insight into how oscillators work and why injection locking happens. Intuitive analytical design techniques are therefore very desirable as preliminary design aids. Over the past several decades, a variety of such techniques have been proposed. Classical techniques such as the well-known Adler [1] and Kurokawa methods [6], and recent follow-ups such as [15], typically rely heavily on linearized analysis. Although such approaches can provide useful insight and intuition into aspects of the phenomenon, they do not directly address the crucial rôle of *circuit nonlinearities* in injection locking. As is well known [14, 17, 18], nonlinearities are crucial for stable oscillator operation as well as for enabling injection locking phenomena in the first place.

Recent work [14, 17] analyzing injection locking relies on using polynomial approximations of circuit nonlinearities for 1-port oscillators. Such nonlinear-centric analyses are much more accurate than prior linear ones; however, the use of polynomial approximations limits accuracy, while also leading to long and complex derivations/formulae, which detract from intuition and insight. To alleviate these issues, a rigorous yet intuitive nonlinear feedback analysis technique, using only simple circuit and mathematical concepts, was proposed in [18] — this technique also provides graphical insights into how nonlinearity plays a role in injection locking. However, the technique applies only to very simple nonlinear negative resistance oscillators, *i.e.*, where the negative resistance is a one-port (two-terminal) element. This limits its practical applicability to only, e.g., tunnel-diode oscillators, which are not in common use today, especially in IC applications. Most integrated oscillators used today involve bipolar transistors or MOS devices, which are 2-port (*i.e.*, 3 or 4 terminal) nonlinear elements.

In this paper, we generalize the technique of [18] to apply to arbitrary two-port nonlinear feedback oscillators. We use the new approach

to rigorously analyse the mechanisms behind stable oscillation and injection locking in the Colpitts oscillator. A key innovation of our technique is the use of *vector nonlinear feedback analysis*. Unlike previous analyses (e.g., [9, 13, 18]) which introduce simplifications such as treating amplitude and frequency components separately, our approach does not ignore coupling phenomena between amplitude and frequency components; indeed, coupling effects are crucially responsible for frequency deviations from idealized oscillation in reality. Our analysis also leads to a new rigorous graphical injection locking prediction procedure which does not rely on approximations (such as polynomial nonlinearities, or the assumption that the oscillator amplitude remains roughly constant due to saturation effects [18] — such approximations are not valid for Colpitts oscillators, as we show). We emphasize that the vector nonlinear feedback analysis developed here is general and can be applied to other two-port nonlinearity based LC oscillators, such as Hartley, Pierce, etc..

The remainder of the paper is organized as follows. In Section II, we develop our vector nonlinear feedback analysis procedure and use it to predict unforced stable oscillations in a Colpitts oscillator. In Section III, we extend this analysis to predict injection locking via a simple but rigorous graphical technique. In Section IV, we present results from applying our approach, compare them against previous approaches, and validate them using simulation.

## II. TWO-PORT NONLINEAR FEEDBACK ANALYSIS FOR OSCILLATION AMPLITUDE AND FREQUENCY

Traditional analysis of oscillator operation is based on a linear feedback loop (e.g., [16]), despite that fact that stable oscillation depends crucially on nonlinearity. This linear feedback analysis in the Laplace domain leads to the relation:

$$Y(s) = \frac{A(s)}{1 - A(s)\beta(s)}X(s) \quad (1)$$

where  $X(s)$  and  $Y(s)$  are the input and output, respectively;  $A(s)$  is the transfer function of an (open-loop) amplifier and  $\beta(s)$  is a feedback factor. The so-called Barkhausen criterion (*i.e.*,  $A(s)\beta(s) = 1$ ) is then used to estimate whether the circuit is able to oscillate. Although this simple criterion provides insights and has long been used in oscillator design, it also has its shortcomings [18]. It provides little information (or even wrong insights) into important issues such as the amplitude of oscillation, the effects of perturbations during oscillation (e.g., injection locking), etc..

Our nonlinear feedback analysis starts from recasting an oscillator as two parts: a nonlinear element and a feedback network. Figure 1(a) shows a simple Colpitts oscillator with all parasitics ignored or lumped within the LC tank (the oscillator's parameters are chosen, in this case, to result in a frequency of roughly 1GHz). We re-interpret the circuit of Figure 1(a) as (crucially) the interconnection of 2 two-port blocks. The first is the RLC tank circuit (including Vdd) as shown by the upper box. The two ports are  $(v_1, i_1)$  and  $(v_2, i_2)$ . For this block, we consider the currents  $[i_1, i_2]^T$  to be the "inputs" and the voltages  $[v_1, v_2]^T$  to be the "outputs", as depicted in the upper block of Figure 1(b). The lower box of Figure 1(a) encapsulates the transistor as well as the emitter degeneration resistor  $R_e$ , as a two-port nonlinear block. For this block, the "input" is  $[v_1, v_2]^T$  and the output is  $[i_1, i_2]^T$ , as shown in the lower block of Figure 1(b). The choice of input and output above is based on the fact that transistors are voltage controlled. Ebers-Moll model [16] of BJT is used in the analysis. Since the BJT works in the cut-off and active regions (CB diode is reverse-biased),  $[i_1, i_2]^T$  are independent of  $v_1$ , thus simplifying the analysis.

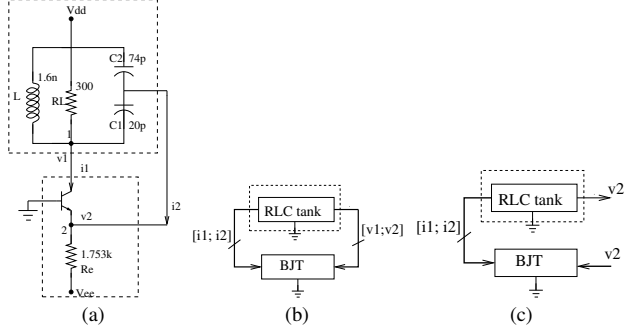


Fig. 1. Block diagram .

Next, we cut the feedback loop on  $v_2$ , as shown in Figure 1(c) (this cut is only conceptual; it is not a physical cut [18], since the currents are connected but the voltages are not). We assume that  $v_2$  is sinusoidal with a DC component, *i.e.*, of the form (this assumption will be justified later)

$$v_2(t) = A_0 + A_1 \sin(\omega_0 t). \quad (2)$$

Then at the output of the 2-port transistor block,  $i_1$  and  $i_2$  are given by (as mentioned early, we ignore the CB diode here)

$$\begin{aligned} i_1 &= d(-v_2), \\ i_2 &= \frac{v_2}{R_e} - \frac{i_1}{\alpha} = \frac{v_2}{R_e} - \frac{d(-v_2)}{\alpha}. \end{aligned} \quad (3)$$

Here, the nonlinear function  $d(\cdot)$  is an exponential  $v$ - $i$  relationship for the base-emitter diode within the BJT [16],  $\alpha$  is common-base current gain. Since  $v_2$  is periodic and the BJT model is memoryless,  $i_1$  (and  $i_2$ ) are also periodic with the same period. Therefore, they can be expressed by Fourier series [12]. We are mainly interested in the fundamental harmonics of  $[i_1, i_2]^T$  since higher harmonics will be filtered out by the RLC tank block, as shown later. We denote the fundamental harmonics of  $i_1$  and  $i_2$  as  $I_{11}(A_0, A_1)$  and  $I_{21}(A_0, A_1)$ , respectively.  $i_1$  and  $i_2$  will also contain significant DC and higher harmonic content due to the strongly nonlinear characteristics of the BJT. In terms of phase characteristics, a memoryless nonlinear element can only contribute a phase shift of either 0 or  $\pi$ .

Now, consider the response of the RLC tank on the input  $[i_1, i_2]^T$ . The input-output relations of the two-port RLC network can be easily derived from:

$$\begin{bmatrix} i_1 \\ i_2 \end{bmatrix} = \begin{bmatrix} \frac{1}{sL} + G_L + sC_1 & -sC_1 \\ -sC_1 & s(C_1 + C_2) \end{bmatrix} \begin{bmatrix} v_1 - V_{dd} \\ v_2 - V_{dd} \end{bmatrix}. \quad (4)$$

We denote the above equation as  $I = GV$ . The transfer function  $\frac{V(s)}{I(s)}$  is the inverse of  $G$  (*i.e.*,  $V = G^{-1}I$ ), denoted as  $Z$ :

$$\mathbf{Z} = \begin{bmatrix} Z_{11} & Z_{21} \\ Z_{21} & Z_{22} \end{bmatrix}. \quad (5)$$

$Z_{12} = Z_{21}$  due to reciprocity of the linear, time-invariant block [11]. Since we only interested in  $v_2$ , we need only consider the amplitude and phase characteristics of  $Z_{21}$  and  $Z_{22}$ . To obtain an intuitive appreciation of these quantities, we plot the amplitude and phase characteristics of  $Z_{21}$  and  $Z_{22}$  in Figure 2 and Figure 3. Observe that at DC (*i.e.*,  $s = 0$ )  $Z_{22}$  is infinity. This implies that the DC component of  $i_2$ , denoted as  $I_{20}(A_0, A_1)$ , is zero:

$$I_{20}(A_0, A_1) = 0. \quad (6)$$

Next, we note that  $Z_{21}$  acts as a filter on  $i_1$  with the amplitude peak at the resonant frequency  $\omega_c = \frac{1}{LC}$  (the value of the peak is  $\frac{C_1}{C_1 + C_2} RL$ ). The amplitude falls down rapidly on both sides. The rate at which  $Z_{21}$  falls down depends on the Q factor of the RLC tank. Even for modest

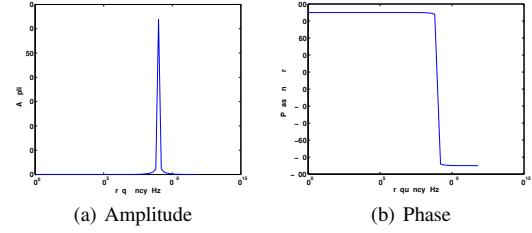


Fig. 2. Amplitude and phase characteristics of the transfer function  $Z_{21}$  ( $V_2$  vs.  $I_1$ ).

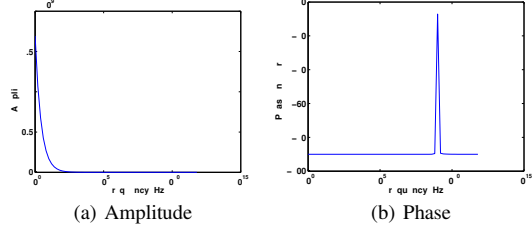


Fig. 3. Amplitude and phase characteristics of the transfer function  $Z_{22}$  ( $V_2$  vs.  $I_2$ ).

Q, all non-fundamental harmonics are filtered to very near zero. At the resonant (fundamental) frequency, the phase characteristic crosses zero rapidly.

On the other hand, the amplitude characteristics of  $Z_{22}$  is infinity at DC but falls quickly as the frequency increases. This implies that  $i_2$  contributes mostly to the DC component of  $v_2$  (DC component of  $i_2$  is zero (6)) but very little to the other harmonics, especially the higher harmonics. The phase features a nonzero peak at the resonant frequency and falls down rapidly on both sides of  $\omega_c$ . The value of this peak depends on the Q factor of the oscillator. For a high-Q oscillator, the value approaches zero; for a moderate-Q factor, this value can, however, be far away from zero (*e.g.*, for a  $Q = 3$  oscillator, this value is around  $-50^\circ$ ). The total effect of the feedback network is the combination of these two:

$$v'_2 = Z_{21}i_1 + Z_{22}i_2. \quad (7)$$

From the above analysis, we justify our original assumption that  $v_2$  in (2) was sinusoidal with a DC component. Furthermore, the frequency of the oscillator ( $\omega_0$ ) has to be close to the resonant frequency ( $\omega_c$ ), but not necessarily exactly equal to it. (If the frequency is too far, the fundamental harmonic is filtered out.) It is now clear why we limit attention only to the fundamental (and DC) components of  $[i_1, i_2]^T$ , since higher harmonics are filtered out. Thus, the fundamental harmonic of the output of RLC tank output is:

$$v'_{21} = 2[I_{11}(A_0, A_1)Z_{21}(\omega_0) + I_{21}(A_0, A_1)Z_{22}(\omega_0)]. \quad (8)$$

To close the loop, we must have  $v'_2 = v_2$  for both amplitude and phase. Thus,

$$A_1 = 2|I_{11}(A_0, A_1)Z_{21}(\omega_0) + I_{21}(A_0, A_1)Z_{22}(\omega_0)| \quad (9)$$

and the phase of  $v'_2$  is zero. Or equivalently,

$$\begin{aligned} \Re(2I_{11}(A_0, A_1)Z_{21}(\omega_0) + 2I_{21}(A_0, A_1)Z_{22}(\omega_0)) &= A_1, \\ \Im(2I_{11}(A_0, A_1)Z_{21}(\omega_0) + 2I_{21}(A_0, A_1)Z_{22}(\omega_0)) &= 0. \end{aligned} \quad (10)$$

As noted previously, the memoryless BJT block only causes a phase shift of 0 or  $\pi$ . Because of its negative resistance nature during intended operation [18], the phase shift of  $i_1$  is  $\pi$  (we do not consider  $i_2$  initially, since it contributes very little to the fundamental, as noted earlier). Also note there is a minus sign for  $i_1$  because the current enters the nonlinear box. Thus, the total phase shift is  $2\pi$ . Therefore the

RLC tank should have a phase shift of 0 for oscillation to result. The phase shift of  $i_1$  at the resonant frequency  $\omega_c$  is exactly 0. However, the phase characteristics of  $Z_{22}$  shows that the phase is not exactly 0 at  $\omega_c$ , especially for low-Q oscillators. It is for this reason that we treat the oscillation frequency as an extra unknown ( $\omega_0$ ) since the deviation from  $\omega_c$  generates some phase shift in  $Z_{21}$  part which compensates the phase shift in the  $Z_{22}$  part (with correct relative amount according to  $I_{11}$  and  $I_{21}$ ), thus making the total phase shift to be 0. This is one of the key differences between our approach and the approach in [18]. This also explains why the oscillator frequency is not exactly  $\omega_c$ , especially for low Q oscillators. As mentioned earlier, the phase shift of  $Z_{22}$  is almost 0 at  $\omega_c$  for high-Q oscillators. Since the amplitude characteristics of  $Z_{21}$  falls down rapidly on both sides of  $\omega_c$ , little deviation from  $\omega_c$ , which is ignored in [18], can cause not-so-small difference in output voltage.

(6) and (10) form an equation system with 3 equations and 3 unknowns. It can be solved numerically by any nonlinear solver, such as Newton's method; however, blind numerical solution does not generate much insight. We now present a graphical approach, which provides much more design insight, to estimate  $A_0$ ,  $A_1$  and  $\omega_0$ .

We first fix a value for  $A_0$  (which we will later sweep over a range). Then, we can first solve for  $A_1$  from (6). The  $A_1$ - $A_0$  relation is plotted in Figure 4 as solid line. The final solution should be on this line. Similarly, with fixed values of  $A_0$ , we also solve for  $A_1$  and  $\omega_0$  from (10). We now have a new  $A_1$ - $A_0$  relations, as shown in Figure 4 in dashed line. The intersection of these two lines satisfies all equations and is the final solution of  $A_0$  and  $A_1$ . The  $\omega_0$  corresponding to these  $A_0$  and  $A_1$  (from (10)) is the oscillator frequency.

We also show the  $A_1$ - $A_0$  relations with different parameters in RLC tank (the first line remains unchanged). As can be seen, the intersection moved to the right as  $R$  goes high. This information can be used to aid oscillator design. More results are shown in Section IV.

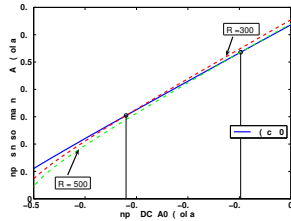


Fig. 4. Solution  $A_1$  and  $A_0$  using nonlinear feedback.

### III. NONLINEAR ANALYSIS FOR INJECTION LOCKING

One of the key benefits of the above nonlinear feedback analysis is that it can be extended naturally to predict injection locking. We inject an external voltage perturbation at  $v_2$ , as shown in Figure 5(a) and Figure 5(b) (current injections can be handled similarly). We assume that the injection signal is a sinusoid of  $v_{inj} = A_i \cos(\omega_i t + \phi_i(t))$ . Here  $\omega_i$  is assumed to be close to the oscillator's natural frequency  $\omega_0$ .

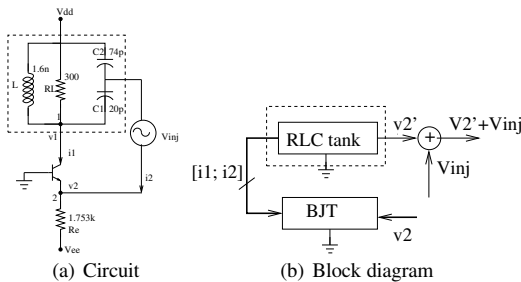


Fig. 5. Colpitts oscillator with voltage injection.

When the oscillator is in lock, it changes its frequency to be the same as the injection signal  $\omega_i$ . This motivates our assumption that

$$v_2(t) = A_0 + A_1 \sin(\omega_i t). \quad (11)$$

Note here that the input frequency is  $\omega_i$ , not  $\omega_0$ .

The nonlinear analysis for the BJT part remains the same as in Section II since it is a memoryless element. In addition, since  $\omega_i$  is very close to  $\omega_0$ , the previous conclusion that higher harmonics are filtered out still holds. We only need to consider DC and fundamental components of the output  $[i_1, i_2]^T$ .

However, the analysis of the feedback network is different from Section II. First, we note that (6) remains true since it derived from the DC value of  $Z_{22}$  (all transfer functions remain the same). From Section II, we know that at exactly  $\omega_0$ , the output  $v_2'$  has an amplitude equivalent to input amplitude ( $A_1$ ) and zero phase shift (or  $2\pi$ ). Then the deviation from  $\omega_0$  (now, the fundamental frequency is  $\omega_i$ ) normally generates a different amplitude and non-zero phase shift. It is the injection signal that compensates for these differences so that the amplitude is exactly  $A_1$  and the phase is exactly zero (or  $2\pi$ ) at the output.

In [2] and [18], a simple graphical approach using phasor diagrams is provided for finding lock range. However, the approach provided in [2] made some simplification by assuming that  $H(\omega_i)I_1(A)$  remains the same when  $A$  changes (i.e., the amplitude at the output of the loop does not change regardless of input amplitude ( $A$ )). Then the minimum amplitude of injection signal needed to lock the oscillator at a fixed locking frequency is easily determined, since it is the perpendicular distance between the tip of  $H(\omega_i)I_1(A)$  and the horizontal axis, as shown in Figure 6. The lock range, the maximum deviation of injection frequency from  $\omega_0$  under certain perturbation strength, can be obtained. However, this assumption is not always true even for the simple negative LC oscillator in [18].

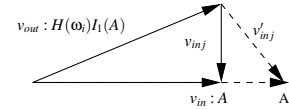


Fig. 6. Phasor diagram

Here, we present a simple but rigorous graphical approach for predicting the lock range of the Colpitts oscillator. In our technique, we fix the injection frequency  $\omega_i$  and estimate the minimum injection amplitude to lock the oscillator. Similar to the technique in Section II, we first fix a value for  $A_0$  and solve for  $A_1$  using (6). The  $A_1$ - $A_0$  relations are the same as in Section II since they do not depend on frequency. The final solution must satisfy these  $A_1$ - $A_0$  relations. With these ( $A_0$ ,  $A_1$ ) pairs, as well as  $\omega_i$ , we can calculate the fundamental harmonics at the output of the loop using (8), as shown in the phasor diagram Figure 7(a). As can be seen, it is not a constant with different ( $A_0$ ,  $A_1$ ) pairs. The input has amplitude  $A_1$  and zero phase shift, as shown in Figure 7(a). Therefore, one input  $A_1$  (hence  $A_0$ , determined from (6)) corresponds to one fundamental harmonics of output  $v_{21}'$  in the phasor diagram Figure 7(a). The difference of the two is the injection signal, as shown in Figure 7(a). Thus, the minimum difference is the minimum injection amplitude. Usually, it is not as predicted by [18] to be perpendicular to the input signal. Figure 7(b) shows the amplitude of this difference as it varies with different inputs  $A_1$ . A minimum can be seen in Figure 7(b), which is minimum injection amplitude. The corresponding  $A_0$  and  $A_1$  are the DC and fundamental components of the input when the oscillator is in lock. More results are shown in Section IV.

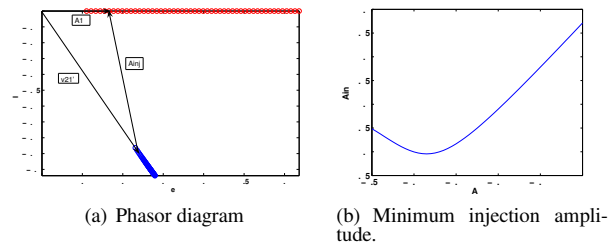


Fig. 7. Predicting injection locking by phasor diagram.

parameters					our method			HB simulation		
R ( $\Omega$ )	L (nH)	C1 (pf)	C2 (pf)	Q	$A_0$ (v)	$A_1$ (v)	$f/f_c$	$A_0$	$A_0$	$f/f_c$
200	1.6	20	74	19.8	-0.424	0.194	1.0013	-0.424	0.195	1.001
300	1.6	20	74	29.7	-0.32	0.305	1.0006	-0.32	0.305	1.0004
500	1.6	20	74	49.5	-0.097	0.536	1.00022	-0.097	0.536	1.00014
1000	1.6	20	74	99	0.544	1.19	1.00006	0.544	1.19	1.00004

TABLE I  
COMPARISON: RESULTS FROM OUR NONLINEAR OUTPUT VOLTAGE ANALYSIS AND HB SIMULATION.

#### IV. VALIDATION

In this section, we first show results from the preceding nonlinear vector feedback analysis (with different circuit parameters), validating against Harmonic Balance (HB) simulation. We also compare the lock range predicted by our technique against full simulation, as well as against Adler's method. We compare corresponding oscillation waveforms obtained via our approach with those from full simulation.

##### A. Free Running Oscillation

Our nonlinear free-running oscillation analysis is tested using the circuit in Figure 1(a). In this experiment, we change the value of R in the RLC feedback network, which changes the Q factor of the oscillator and the characteristics of the feedback network. Table I shows the results from our analysis. For comparison, we also show the results from HB simulation, which is used to solve oscillator steady state. As can be seen, they are in good agreement. Also, it verifies our conclusion in Section II that the oscillator frequency is not exactly  $\omega_c$  ( $\omega_c = 2\pi f_c$ ), especially for low-Q oscillators.

##### B. Injection Locked Oscillation

In this experiment, we fix R to be 500 (all other parameters remain the same as in Figure 1(a)), resulting in a Q factor of about 50. The perturbation is a voltage source connected as in Figure 5(a). Figure 8 shows the lock range predicted by our technique, compared with full simulations (first using transient simulation and then refining the results by HB). As can be seen, they match almost perfectly. In addition, we also show results from Adler's equation, which is based on linear simplifications and is over-conservative [18].

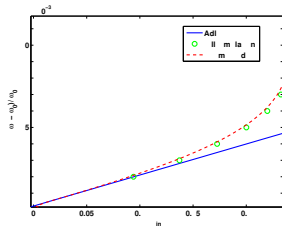


Fig. 8. Lock range: Adler, our method, full simulation.

We also show corresponding output voltages when the oscillator is in lock perturbed by the injection signal predicted above. We verify the results by full simulation, as shown in Figure 9. Another approach similar to [18], in which injection signal is estimated to be perpendicular to the input, is also tested. The result is also shown in Figure 9. It does not match full simulation well.

#### V. SUMMARY

We have presented a simple but rigorous technique for understanding and predicting free-running and injection-locked oscillation in two port nonlinear resistance oscillators, such as Colpitts. Our approach employs vector-based nonlinear feedback analysis which can be interpreted and implemented in a graphical way. We have validated our technique against transient and HB simulations, demonstrating agreement considerably superior than previous approaches. Our analysis is general and can be extended to other LC oscillators, such as Pierce, Hartley, etc., oscillators.

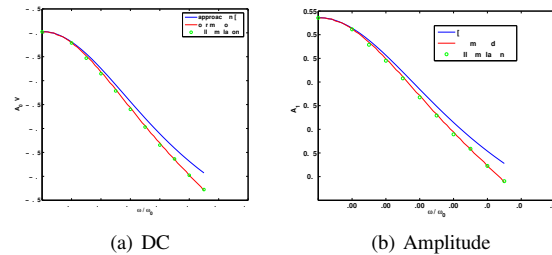


Fig. 9. Output voltage: our method, full simulation, approach in [18].

#### REFERENCES

- [1] R. Adler. A study of locking phenomena in oscillators. *Proc. Inst. Radio Eng.*, 34:351–357, Jun 1946.
- [2] University of Minnesota Analog System Verification Group. <http://laoo.dtc.umn.edu/jr/code/injlock>.
- [3] A. Demir and J. Roychowdhury. A Reliable and Efficient Procedure for Oscillator PPV Computation, with Phase Noise Macromodelling Applications. *IEEE Transactions on Computer-Aided Design of Integrated Circuits and Systems*, pages 188–197, February 2003.
- [4] Prashant Goyal, Xiaolue Lai, and Jaijeet Roychowdhury. A fast methodology for first-time-correct design of plls using nonlinear phase-domain vco macromodels. In *Proceedings of the 2006 conference on Asia South Pacific design automation*, pages 291–296, 2006.
- [5] P. Kinget, R. Melville, D. Long, and V. Gopinathan. An injection-locking scheme for precision quadrature generation. *IEEE Journal of Solid-State Circuits*, 37:845–851, 2002.
- [6] K. Kurokawa. Injection locking of microwave solid-state oscillators. *Proc. IEEE*, 61:1336–1410, Oct 1973.
- [7] X. Lai and J. Roychowdhury. Automated oscillator macromodelling techniques for capturing amplitude variations and injection locking. In *Proc. IEEE ICCAD*, Nov 2004.
- [8] X. Lai and J. Roychowdhury. Capturing Oscillator Injection Locking via Nonlinear Phase-Domain Macromodels. *IEEE Trans. Microwave Theory Tech.*, 52(9):2251–2261, Sep 2004.
- [9] K. Mayaram. Output voltage analysis for the mos colpitts oscillator. *IEEE Trans. Ckts. Syst. – I: Fund. Th. Appl.*, 47(2):260–263, 2000.
- [10] T. Mei and J. Roychowdhury. Oscillator-AC: Restoring Rigour to Linearized Small-Signal Analysis of Oscillators. In *Proc. IEEE ICCAD*, pages 604–609, 2005.
- [11] Chua L. O., C. A. Desoer, and E. A. Kuh. *Linear and Nonlinear Circuits*. McGraw-Hill, INC, New York, 1987.
- [12] A. Papoulis. *Signal analysis*. McGraw-Hill Press, INC, New York, 1997.
- [13] D. Pederson and K. Mayaram. *Analog integrated circuits for communication: principles, simulation and design*. Kluwer Academic Publishers, 1991.
- [14] H. Rategh and T. Lee. Superharmonic injection locked frequency dividers. *IEEE J. Solid-State Circuits*, 34:813–821, June 1998.
- [15] B. Razavi. A study of injection locking and pulling in oscillators. *IEEE J. Solid-State Circuits*, 39:1415–1424, September 2004.
- [16] Adel S. Sedra and Kenneth C. Smith. *Microelectronic circuits*. Oxford University Press, INC, New York, 4 edition, 1998.
- [17] S. Verma, H. Rategh, and T. Lee. A Unified Model for Injection-Locked Frequency Dividers. *IEEE J. Solid-State Circuits*, 38:1015–1027, June 2003.
- [18] X. Lai Y. Wan and J. Roychowdhury. Understanding injection locking in negative-resistance lc oscillators intuitively using nonlinear feedback analysis. In *Proc IEEE Custom Integrated Circuits Conference*, pages 729–732, 2005.